Visualization on Turbulent Flow structure in 19-Pin SFR Wire-wrapped Fuel Bundle: Preliminary Analysis

Min Seop Song [a], Jae Ho Jeong [b], Eung Soo Kim[a*]
[a]*Department of Nuclear Engineering, Seoul National University, 559 Gwanak-ro, Gwanak-gu, Seoul, South Korea*
[b]*Korea Atomic Energy Research Institute 989-111 Daedeok-daero, Yuseoung-gu, Daejeon, Republic of Korea*
[*]*Corresponding author: kes7741@snu.ac.kr*

1. Introduction

Sodium-cooled Fast Reactor (SFR) is one of the 4th generation reactors that utilizes sodium as a coolant. The core of SFR consists of wire-wrapped fuel bundle where wires prevent collisions and maintain the interval between rods. Compared to bare rod bundles, wire makes the flow in the fuel bundle more complicated by inducing transverse flow and separation flow. Therefore, there have been efforts for experimentally investigating complex velocity field in wire-wrapped fuel bundle with flow visualization techniques [1,2]. However, complex geometry and optical distortion have been obstacles for flow visualization. The previous researches provided solutions by matching indices of refractions of a model and working fluid they used, but it still needs more experimental results for various cases because it inherently contains uncertainty due to geometry and experimental methods.

This study describes a construction process of the experimental facility for the flow visualization in 19 wire-wrapped rod bundle and its experimental result with 2D particle image velocimetry system. The measurement data at the edge and interior subchannels will be presented in detail to understand the average flow field and turbulent flow structures.

2. Flow Visualization Experiments in Wire-wrapped Pin Bundle

2.1 SNU 19-Pin Wire-wrapped Rod Bundle

The geometry of wire-wrapped fuel bundle is complex because wire attached to rod continuously changes cross sectional area in the fuel bundle. And wire itself makes small gap that increase refractions. Therefore, flow visualization in this geometry is hard. A matching refractive index (MIR) technique can be helpful to minimize distortions. Our research group have developed MIR technique using 3D-printing and rapid prototyping model and herb oils [3]. In this experiment, a transparent epoxy model was fabricated based on the master model of PVC with vacuum casting process (Fig. 1). A mold was made from the elaborately crafted master model. And the mold replicated 19 identical replicas. This process enables to create models of the same shape with less tolerances. The refractive index of epoxy is 1.555 at the wavelength of 532nm. Therefore, pure anise oil was used to match the refractive index [3]. The density and viscosity at the experimental condition (34℃) is 982kg/m^3 and 0.734mPas.

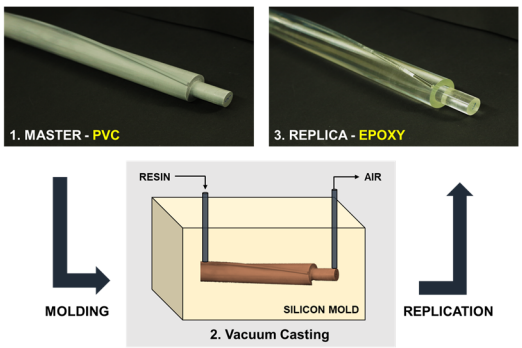

Fig. 1. A fabrication process of the epoxy replica with vacuum casting

Fig 2 shows the overall configuration of the SNU 19-pin wire-wrapped rod bundle facility. It is a closed loop system that is designed to have chemical resistance. In the test section, the flow develops from bottom to top for the length of four rotation (1.848m). For the three rotations, wire-wrapped rods made of SUS are used, and the last one rotation is composed of epoxy model for visualization. The wire and rod diameter is 3mm, 20mm each, and the distance between rod is 24mm.

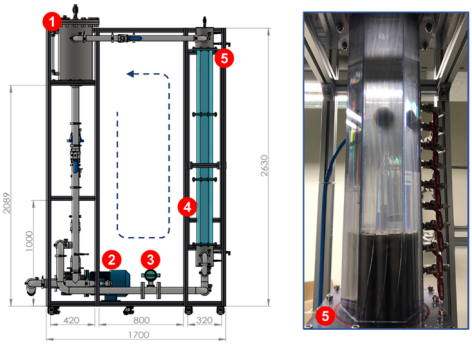

Fig. 2. A configuration of SNU 19-Pin wire-wrapped rod bundle and test section image (1: Tank, 2: Pump, 3: Turbine Flow Meter, 4: Test Section (SUS Rod), 5: Test Section (Vacuum Casting Rod).

2.2 Particle Image Velocimetry Setup

Particle Image Velocimetry (PIV) was used to visualize the flow inside of test section. The PIV system is composed of a camera, laser with optics and synchronizer that controls the timing precision of camera and laser generator. In this experiment, one CCD camera (PCO1600) and Nd:Yag Laser (532nm) were used to

obtain 2D-velocity fields. The fluorescent particles that emit light of 580nm from the 532nm were seeded in the working fluid to separate particle image from the laser sheet. The time interval between image frames was 200um with a flow rate of 303LPM. Reynolds number at this flow rate is about 16,500 which is expected in the turbulent regime. [4] The size of the interrogation area was 24x24 with 50% overlap. The particle images were enhanced with background removal and high-pass filtering. The velocity field was calculated with multi-pass cross-correlation algorithm.

PIV measurements were made in 15 locations with five planes in the y-direction and three planes in the z-direction. Two thousand image pairs were collected for each measurement. Figure 3 shows the measurement planes in the y-direction. Plane 1 and 2 belong to the outmost region (edge subchannels). Plane 3,4 and 5 are placed in interior subchannel where different flow structure is made. Laser sheet was inserted from the right side through triangular oil jacket to keep the path of laser unchanged. The measurement plane for z-direction is described in figure 4. The z-position of the test section is related to the wire-phase. Based on the z= 1.386 where the wire located in right side of the rod, the planes in z-direction shows a variation of the flow field when wire rotates about 180 degrees. In this region, large edge vortex and small interior vortex are repeatedly made. [5]

In this study, Planes 1,3 in the y-direction at the first location in z-direction was preliminarily analyzed.

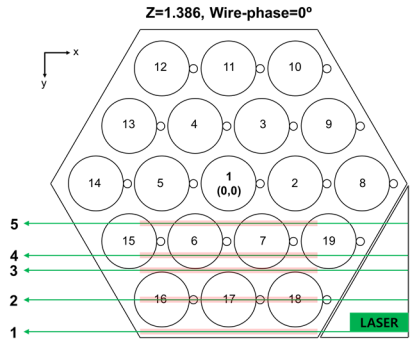

Fig. 3. PIV Measurement Planes (1: Y=-0.0535m, 2: -0.0415m, 3: -0.0312m, 4: -0.0271m, 5: -0.0145m.)

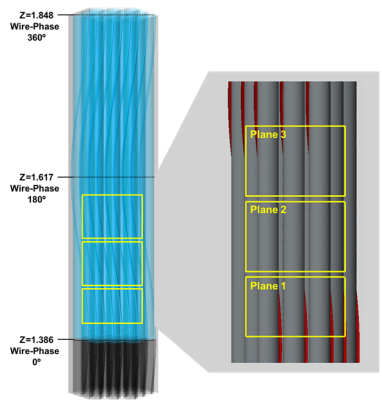

Fig. 4. PIV measurement planes in z-direction. (Plane 1: Z=1.396~1.451m, Plane 2: 1.456 ~ 1.521m and Plane 3: 1.526~1.591m.)

3. Flow Field Measurement Result and Discussion

Flow fields in each measurement planes were obtained from the ensemble-average of 2,000 instantaneous velocity fields. The statistical convergence of average velocity data, distribution of velocity component and turbulent structure from two-point velocity correlations were analyzed.

3.1 Convergence of Data

The convergence of velocity components is calculated as a relative error between average velocity for a finite number of frames (N_f) and the total average value ($N_f = 2{,}000$). Turbulent behavior of flow makes the velocity components continuously fluctuate. With assumptions that the time interval between PIV images is longer than twice integral time scale and that the random fluctuation is higher than the PIV uncertainty, the standard deviation of $\tilde{\bar{u}}$ in Eq. 1 follows the trend of $N_f^{-0.5}$. [6]

Figure 5 shows the convergence results. Both components in each measurement points show converged trends after 500 image pairs. The relative error of u was higher than the v because of the small absolute value of average u.

$$\tilde{\bar{u}} = \frac{1}{N_F}\sum_{n=1}^{N_F} \tilde{u}_n \qquad (1)$$

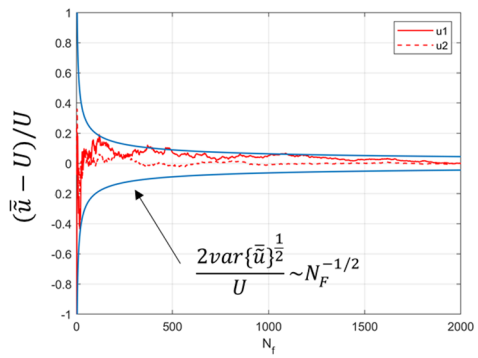

(a) u-component

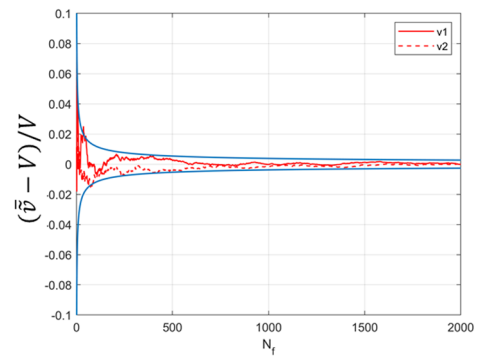

(b) v-component

Fig. 5. Difference between measured mean U, V over finite number of images (N_f). (x1,y1: 0.31m, 1.389m, x2,y2: 0.31m, 1.451m)

3.2 Velocity Field and Turbulence Structures

Distribution of average velocity in x, z-direction, streamline and spatial correlation plots are presented in figure 6. The velocity field in P1 shows the flow distribution at the edge vortex. This location in edge subchannel was found that the large edge vortex is made when the axial flow separates from the wire [5]. The PIV result also shows a repetitive variation of u component due to vortex formation at the 1400mm. The vortex at the x=10mm is maintained to the 1440mm. The axial velocity in the vortex region shows a higher value than others indicating that the vortex induced higher axial velocity [5].

The velocity field at P3 also shows the repetitive variation of u component due to the vortex in the interior subchannel. These vortices are developed from the wire of Rod 16 and 17. As the wire turns into the interior region between rod 7, 17 and 18, vortex induced accelerate the axial velocity. The magnitude of axial velocity was higher to the right. The high axial velocity between x=0 ~ 10mm seems to be a small distortion of the flow field due to a bonded area between replica and SUS.

Streamlines show that u velocity at the edge subchannel develops at the higher z. This is a swirl flow at the edge subchannel [5].

PIV result of instantaneous velocity fields provides a spatial distribution of velocity components at the same time. This enables to investigate turbulent structures in the flow field with the high-order correlation function. Especially, the spatial distribution of 2nd momentum of velocity component contains information of energy spectral distribution and length scale of turbulent structures. The spatial correlation of velocity fields for the distance d is calculated as Eq 2. [6] The cross-correlation between two fluctuating velocity components are normalized with autocorrelation at the reference point and end of distance vector. Also, the integral length scale of each spatial correlation that represents large turbulence scale are calculated as integral of spatial correlation along each axis directions as Eq 3.

$$R_{u_i u_j}(x_r, d) = \frac{\langle u_i'(x_r) u_j'(x_r+d) \rangle}{\sqrt{\langle u_i'^2(x_r) \rangle} \sqrt{\langle u_j'^2(x_r+d) \rangle}} \quad (2)$$

$$L = \int_0^\infty R_{u_i u_j}(r) dr \quad (3)$$

To investigate spatial correlation distribution, 3 reference points are selected along the line of x=11.35mm. Total integral length scales are listed in Table I. The 2D distribution of spatial correlation results are plotted in figure 6-(e) to (h) for each velocity components. Every contour is clipped at the 0.1 to represent a positively correlated region. For R_{uu}, the contour expanded in u-direction as z increases in plane 1. It is related to the development of swirl flow and break of the vortex. In addition, the spatial correlation shows higher integral length scale in negative direction. Compared to plane 3, the integral length scale in plane 1 is larger, which is related to the size of vortex developed in each subchannel. In terms of R_{vv}, both planes have spatial correlation area expanded in the z-direction as flow develops.

Figure 7 represents spatial correlation plots at reference points in x, z-direction. Even though the x and z-axis are not complete homogeneous directions, it was found that u and v are mostly correlated in reference axis in figure 6. Except for R_{uu} in plane 1, the spatial correlation results have symmetric features. Larger integral length scale in axial direction indicates that it has larger turbulence structures in the axial direction.

4. Conclusions

The construction of SNU 19-Pin Wire-wrapped rod bundle and analysis of PIV experiment result in the test section was discussed. The test section of the experimental facility was built with the epoxy replica to precisely imitate wire-wrapped fuel bundle. The pure

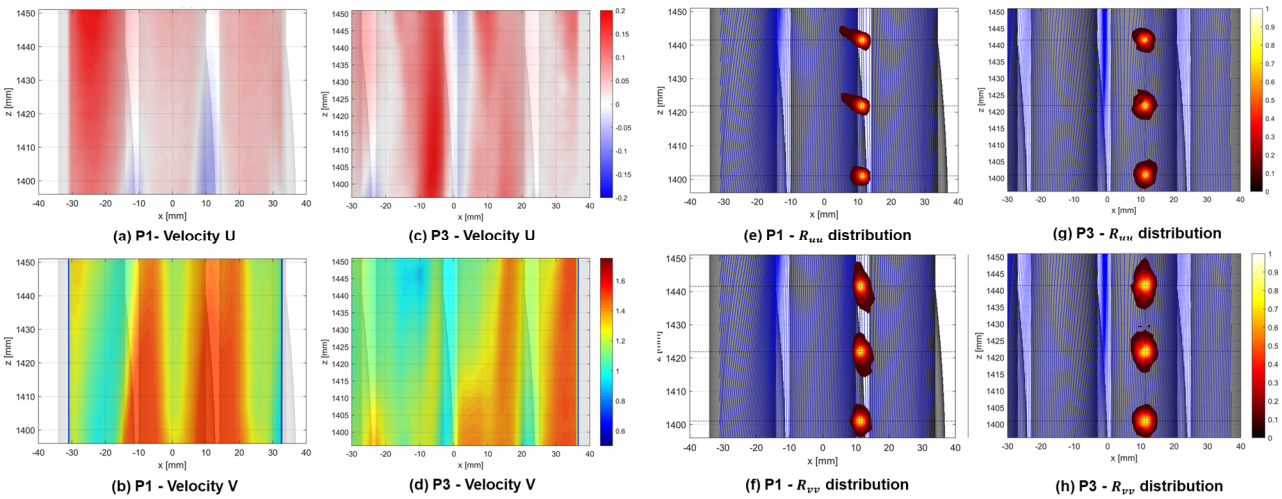

Fig. 6. Contours of velocity field in x, z direction with streamline and spatial correlation result

anise oil was used as a working fluid to minimize optical distortion. From the PIV measurement experiments, velocity field at the edge and interior subchannel were obtained. The velocity field revealed the two major flow patterns in each subchannel; swirl flow and vortex flow. The two-point velocity correlation analysis was conducted to obtain an integral length scale of turbulent flow. From this analysis, the order relation of integral length scales in each direction and location were obtained. Result also shows that the integral length scale changes according to the flow pattern.

We will process the remain PIV data for each measurement plane for further analysis. The flow pattern related to wire position will be investigated in detail. Comparative studies with CFD data will be conducted with uncertainty analysis.

Table I: Integral Length Scales

Location	Integral Length Scale [mm]	
	Plane 1	Plane 3
uu_p1 left	2.123	1.742
uu_p1 right	1.427	1.270
uu_p2 l	2.453	1.757
uu_p2 r	1.210	1.575
uu_p3 l	2.325	1.393
uu_p3 r	1.131	1.402
vv_p1 l	2.714	2.670
vv_p1 r	2.846	2.721
vv_p2 l	3.103	3.165
vv_p2 r	2.437	3.590
vv_p3 l	3.107	3.314
vv_p3 r	3.331	3.513

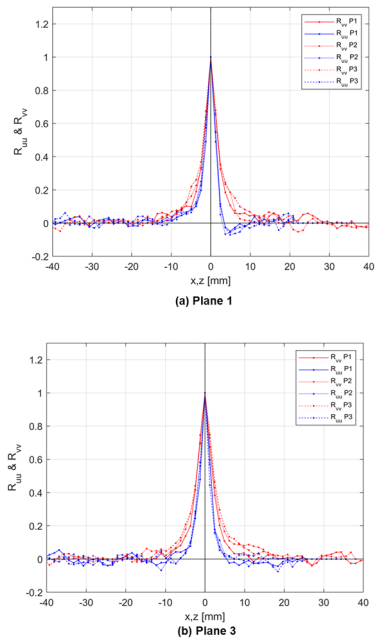

Fig. 7. Spatial correlation plot at the reference points in plane 1 and 3.

ACKNOWLEDGEMENTS

This research was supported by National R&D Program through the National Research Foundation of Korea (NRF) funded by the Ministry of Science, ICT & Future Planning (No. 2016M2B2A9911846)

REFERENCES

[1] M. Nishimura, H. Sato, H. Kamide, H. Ohshima, K. Nagasawa, and Y. Imai, Investigation on Velocity Distribution around the Wrapping Wire in an Inner Subchannel of Fuel Pin Bundle. In ICONE20. California, USA, 2012

[2] N. Goth, P. Jones, T. Duy, R. Vaghetto, Y. Hassan, N. Salpeter, and E. Merzari, PTV / PIV measurements of turbulent flows in interior subchannels of a 61-pin wire-wrapped hexagonal fuel bundle. International Journal of Heat and Fluid Flow, 71, 295–304. 2018

[3] M. S. Song, H. Y. Choi, J. H. Seong, and E. S. Kim, Matching-index-of-refraction of transparent 3D printing models for flow visualization. NED, 284, 185–191.2015

[4] S. K. Chen, N. E. Todreas, and N. T. Nguyen, Evaluation of existing correlations for the prediction of pressure drop in wire-wrapped hexagonal array pin bundles. NED, 267(12. 2013), 109–131. 2014

[5] M. S. Song, J. H. Jeong, E.S. Kim, Numerical Investigation on Vortex behavior in Wire-wrapped Fuel Assembly for a Sodium Fast Reactor, NET, 2018

[6] R. J. Adrian, and J. Westerweel, Particle image velocimetry (No. 30). Cambridge University Press . 2011